Collective Thomson scattering experiments on a tin vapor discharge in the prepinch phase

E. R. Kieft,* J. J. A. M. van der Mullen,† and G. M. W. Kroesen
Department of Applied Physics, Eindhoven University of Technology, P. O. Box 513, 5600 MB Eindhoven, The Netherlands

V. Banine
ASML Netherlands B.V., De Run 6501, 5504 DR Veldhoven, The Netherlands

K. N. Koshelev
ISAN, Troitsk, Moscow Region 142092, Russia
(Received 18 June 2004; published 30 November 2004)

Partially collective Thomson scattering measurements have been performed on a triggered vacuum arc in tin vapor, which is a candidate source of extreme ultraviolet light for application in semiconductor lithography. In this paper, results on the electron densities and temperatures are presented for the prepinch phase of the discharge. Electron densities and temperatures increase from 1×10^{23} m^{-3} to 1×10^{24} m^{-3} and from 5 eV to over 30 eV, respectively, in about 100 ns. The results are confirmed by Stark broadening data.

DOI: 10.1103/PhysRevE.70.056413 PACS number(s): 52.25.Os, 52.70.Kz, 52.80.−s

I. INTRODUCTION

Extreme ultraviolet (EUV) lithography tools that are currently under development for application in the semiconductor industry require high-intensity sources of light in a wavelength band of 2% around 13.5 nm. In recent years, discharge plasmas have been regarded as the most promising candidates to meet the requirements set by the industry, and various types have been investigated by different groups worldwide. In particular, discharges in xenon have received much attention. More recently, increased effort has been put into the development of discharges in tin vapor, since tin has the advantage over most other elements under consideration in that its EUV spectrum is strongly peaked at the desired wavelength (several contributions in [1]).

A triggered vacuum arc in Sn vapor from the Russian Institute of Spectroscopy (ISAN) has been in operation in the ASML EUV laboratory in Veldhoven, The Netherlands since March 2003. The discharge region consists of a flat cathode that is covered with a thin layer of liquid tin, and a ring-shaped anode located a few mm above the cathode. A schematic picture of the electrode cross section is given in Fig. 1. Before the start of the discharge, a positive electrical potential of 4 kV is applied to the anode. The discharge is started by the creation of a cloud of partly ionized tin vapor above the surface of the cathode, which expands towards the edges of the anode. Once the plasma near the anode has reached a sufficiently high density, a discharge starts. The current through the discharge increases to almost 20 kA in only a few tens of ns, and a multiply ionized, EUV-emitting plasma is formed. The strong current causes a pinching effect, meaning that due to Lorentz forces acting on the charged particles in the plasma, the plasma is compressed in the radial direction to a needlelike shape on the axis of the discharge, with a diameter on the order of 100 μm. In view of the dynamics of the plasma, the time development of the discharge can be roughly split up into four main phases: (i) the trigger plasma, before the discharge current has started; (ii) the prepinch phase, in which the plasma is heated and ionized by the strong electrical current, and starts to compress; (iii) the pinch itself; and (iv) a decay phase. Since the pinch phase is very short-lived compared to the other phases of the discharge, its center is suitable to serve as a zero on the time scale when one is describing the properties of the plasma in the other phases.

The various phases of the discharge have been characterized by using time-resolved EUV and visible light imaging and EUV spectrometry, in a similar way to that described in [2] for a hollow cathode discharge in xenon. First results have been presented in [3]; a publication of a more detailed description of the results is underway [4].

The above-mentioned passive imaging and spectroscopic techniques have given valuable information on the qualitative behavior of the discharge. Plasma imaging has confirmed the identification of the four phases mentioned above and revealed details of the plasma evolution within these

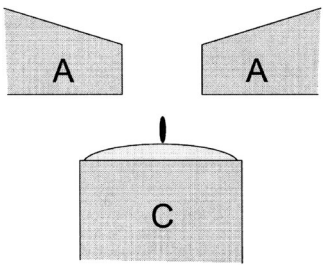

FIG. 1. A schematic cross section of the electrodes of the tin vapor discharge, displaying the anode with a central hole in it (*A*) and the cathode (*C*), covered with a thin layer of liquid tin. The small, elongated shape in the center represents the approximate position of the pinch plasma.

*Electronic address: e.r.kieft@tue.nl
†Corresponding author; electronic address: j.j.a.m.v.d.mullen@tue.nl

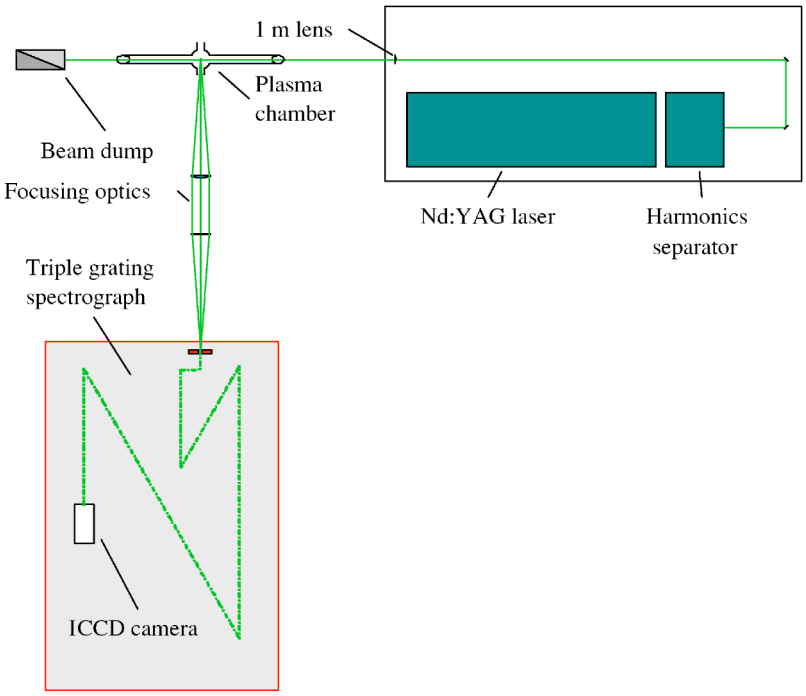

FIG. 2. Top view of the experimental setup for Thomson scattering.

phases. EUV spectroscopy has shown the appearance of various ionization stages of tin (from 7+ to 10+) one after another during the prepinch phase, and the apparent cooling of the plasma during the pinch phase. A drawback of these methods, however, is that they do not give direct information on electron densities and temperatures, which are "fundamental" parameters for understanding and modeling plasmas. Instead, extensive approximations and assumptions (e.g., on the deviations from equilibrium in the plasma) are required to derive these parameters from the experimental results.

A method that can give direct information on both electron densities and temperatures is Thomson scattering (TS) spectroscopy. In this technique, a laser pulse is fired through the plasma, and the spectrum of the laser light scattered from free electrons in the plasma is recorded. In the noncollective scattering limit, the electron density in the plasma can be derived from the total intensity of the Thomson scattered light, whereas the width of the spectrum, caused by the Doppler effect, gives information on the velocity distribution, and hence on the temperature, of the electrons in the plasma. For higher electron densities, corrections for collective scattering need to be made.

In the work presented here, the Thomson scattering technique has been tested for the various phases of the discharge. Until now, we have been able to produce good data only for the prepinch phase. In the other phases, the extraction of good Thomson spectra was impossible due to the relatively high levels of plasma background radiation.

In addition, the measurement of Stark broadening of plasma lines is a frequently used method to determine electron densities in the plasma in a passive way. A few Sn lines in the wavelength range of interest for Thomson scattering were found to be broadened well beyond the apparatus spectral resolution, and the linewidths were used to derive electron density information. Here, this information is used only as a check on the validity of the TS results. A more detailed discussion of the Stark broadening results will be given elsewhere.

In the following section, the collective Thomson scattering theory and experiment will be discussed. After that, the results for the prepinch phase of the discharge are presented. Finally, a possible approach will be discussed for making the TS technique feasible for the other phases of the discharge.

II. COLLECTIVE THOMSON SCATTERING

The setup used for the TS measurements was basically the same as the one described extensively in [5]. It has been used in the past for diagnostics on a range of laboratory plasmas, as described in [5] and, e.g., in [6–8]. A schematic overview of the setup is shown in Fig. 2.

The Thomson scattered photons originated from a frequency doubled Nd:YAG (yttrium aluminum garnet) laser pulse of 7 ns duration, operated at a reduced repetition rate of 5 Hz, with an incident wavelength of $\lambda_i = 532.0$ nm, which was focused into the plasma through a plano-convex lens with a focus length $f = 1$ m. A pulse energy of 170 mJ was applied. Due to certain losses at the optics, effectively about 160 mJ of pulse energy was delivered into the plasma. Brewster-angle entrance and exit windows and a diaphragm just outside the entrance window helped to minimize stray light originating from the vacuum chamber. The laser beam passed through the discharge region between the anode and the cathode; the laser focus was aligned approximately 0.5 mm above the center of the cathode surface. This is the region where the most interesting features of the discharge (such as the trigger plasma and the pinch) occur. As the laser passed through the plasma in a horizontal direction, horizontal profiles of the plasma parameters could be derived from the measurements.

A triple grating spectrograph (TGS) was used to image the light scattered by free electrons inside the plasma onto

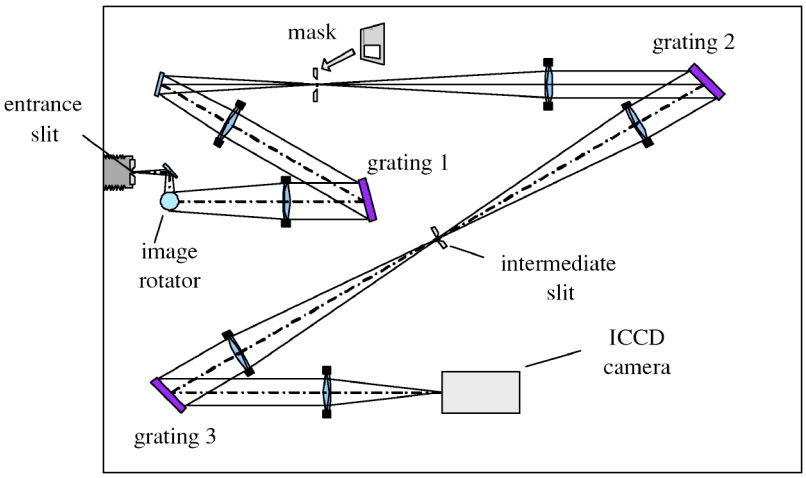

FIG. 3. A schematic view of the triple grating spectrograph as used in this work. The first two spectrographs in subtractive configuration serve as a powerful stray light filter.

the entrance plane of an intensified charge-coupled device (ICCD) camera. An image rotator is located inside the TGS so that horizontal spatial information is imaged onto the camera in the vertical direction. In this way, horizontal cross sections of the plasma parameters can be made and wavelength dispersion can take place in the horizontal plane. The first and second spectrographs are arranged in a subtractive configuration. An important role is played by a mask between the first and second spectrographs, which greatly reduces the Rayleigh scattered signal from the plasma and the stray light due to reflections from surfaces near the probed plasma volume.

The optical gate of the ICCD camera was reduced to 5 ns to minimize the level of background radiation emitted by the plasma itself. For each measurement, the signals from 250 pulses, recorded in 50 s, were added, mainly with the aim of averaging out fluctuations in the background radiation emitted by the plasma.

In the standard configuration of the TGS, the central wavelength was imaged onto the center of the CCD camera, so that a wavelength range of 10.9 nm was recorded. In this way, both sides of the TS spectrum could be recorded up to just over 5 nm away from the central wavelength. This configuration was chosen in the past for the recording the spectra of relatively cool plasmas with a sufficiently good spectral resolution. However, it was less suitable for application in plasmas with higher electron temperatures and/or densities. Therefore, compared to this standard configuration, the last lens in the TGS, the second lens of the third spectrograph, was replaced by one with a focal length $f=300$ mm instead of the 600 mm focal length of the other lenses. Also, the alignment of the gratings was adjusted to project the incident wavelength onto the edge of the covered range instead of onto the center. Accordingly, the mask between the first and second spectrographs was replaced by an edge filter. Depending on which side of the spectrum was selected, a wavelength range of 511.7–531.5 nm or 532.6–552.9 nm could now be covered. A schematic view of the TGS is given in Fig. 3.

The trigger of the discharge, the Q-switch of the TS laser, and the optical gate of the ICCD camera were all synchronized to a flash-lamps-synchronized output from the TS laser, using two Stanford DG 535 delay generators. The relative jitter between the TS laser and the camera was on the order of 1 ns (mainly due to the laser), whereas the jitter of both relative to the plasma was on the order of 5 ns, due to pulse-to-pulse fluctuations in the timing of the start of the discharge after the trigger. These fluctuations, combined with the optical gate time of the camera, put a limit to the time resolution of the measurements.

A rotatable polarization filter was mounted onto the front of the TGS, and the polarization filter on the camera itself was removed. Both the horizontally and the vertically polarized signals were recorded in the presence of the TS laser pulse. The horizontally polarized signal was used to subtract the plasma background from the vertically polarized signal that contained the TS spectrum. This method was used to eliminate any influence of laser heating on the plasma background signal.

For the plasma parameters expected inside an EUV discharge, the TS spectrum would be partially collective. Here, the term *collective* refers to the fact that the free electrons in the plasma respond collectively to the incident laser light; another frequently used name for this type of scattering is coherent Thomson scattering. For fitting the experimental curves, the expression for the collective Thomson spectrum as given by Salpeter [9] was used. The spectral intensity per solid angle is given by

$$\frac{dP_s(\omega)}{d\Omega} = \frac{d\sigma}{d\Omega} P_L L_s n_e S(\mathbf{k},\omega) \tag{1}$$

with P_s the scattered intensity, P_L the incident laser intensity, L_s the length over which scattered light is collected, and σ the single-electron scattering cross section. $\mathbf{k}$ and ω are the scattering wave vector and the angular frequency of the laser light, respectively. The so-called *form factor*, $S(\mathbf{k},\omega)$, is given by

$$S(\mathbf{k},\omega)\mathrm{d}\omega = \frac{1}{\sqrt{\pi}}\Gamma_\alpha(x_e)dx_e + Z\left(\frac{\alpha^2}{1+\alpha^2}\right)^2 \frac{1}{\sqrt{\pi}}\Gamma_\beta(x_i)dx_i, \tag{2}$$

where

$$\Gamma_\alpha(x_e) = \frac{\exp(-x_e^2)}{|1+\alpha^2 W(x_e)|^2},$$

$$\Gamma_\beta(x_i) = \frac{\exp(-x_i^2)}{|1+\beta^2 W(x_i)|^2},$$

$$\beta^2 = Z\left(\frac{\alpha^2}{1+\alpha^2}\right)\frac{T_e}{T_i},$$

$$W(x) = 1 - 2x\exp(-x^2)\int_0^x \exp(p^2)dp - i\sqrt{\pi}x\exp(-x^2). \tag{3}$$

Here, $x_e = \omega/(kv_e)$ and $x_i = \omega/(kv_i)$, with the electron and ion mean thermal speeds, respectively, defined as

$$v_e = \sqrt{\frac{2k_BT_e}{m_e}},\ v_i = \sqrt{\frac{2k_BT_i}{m_i}},$$

where k_B is the Boltzmann constant and $T_{e,i}$ and $m_{e,i}$ are the electron and ion temperatures and masses, respectively. Further, Z represents the average ionization degree and $\alpha = 1/k\lambda_D \sim \sqrt{n_e/T_e}$ is the *scattering parameter* (where λ_D stands for the Debye length of the plasma).

In Eq. (2), the first term represents the so-called *electron contribution*, whereas the second is known as the *ion contribution*. In this work, only the electron contribution has been studied since the ion contribution is so narrow and close to the incident wavelength that it cannot be separately measured and resolved spectrally. The shape of the electron contribution is governed by the scattering parameter α, of which the square appears as a prefactor of the plasma dispersion function $W(x)$ in the denominator of the shape function $\Gamma_\alpha(x)$.

The real part of $W(x)$ contains an integral function that cannot be expressed in closed analytical form, and this is impractical in the actual fitting procedure. Therefore, an approximation $W'(x)$ of $W(x)$ was constructed, with $\mathrm{Im}[W'(x)] = \mathrm{Im}[W(x)]$ and

$$\mathrm{Re}[W'(x)] = -\frac{1}{2x^2} - \frac{3}{4x^4} + \left(\frac{15}{8} + \frac{5}{4x^2} + \frac{3}{4x^4}\right) \times \exp(-x^2) - 0.612x^2\exp(-0.8913x^2) - [0.0038x\sin(3.2x) + 0.0015x^4]\exp(-0.4x^2). \tag{4}$$

This leads to the definition of

$$\Gamma'_\alpha(x_e) = \frac{\exp(-x_e^2)}{|1+\alpha^2 W'(x_e)|^2} \tag{5}$$

which was used instead of $\Gamma_\alpha(x_e)$ for the calculation of $S(\mathbf{k},\omega)$. In this approximation, the generated Thomson spectrum was found to be accurate to better than 0.1% of the peak value for $\alpha \leqslant 1.5$ and 1% or better for $\alpha < 3$. As an example, Fig. 4 shows a plot of $\Gamma_\alpha(x_e)$ for $\alpha = 1.5$, together with a 1000 times magnified plot of the difference $\Gamma'_\alpha(x_e) - \Gamma_\alpha(x_e)$.

In the partially collective regime, α and T_e can be determined from just the shape and the width of the spectrum, respectively. Once both α and T_e are known, n_e can be calculated. Therefore, an absolute calibration of the signal is in principle unnecessary. However, in the present work an intensity calibration of the scattered signal was done by measuring the Raman scattered signal from nitrogen at atmospheric pressure. In the fitting procedure, α was treated as a function of n_e and T_e. In total, three free parameters were used: n_e, T_e (from which two α was calculated), and a third parameter ξ, set to be the ratio of the measured TS intensity and the theoretical one. The value of ξ, which would be equal to 1 in the ideal case, was used as a check of the validity of the results and for evaluating the stability of the source.

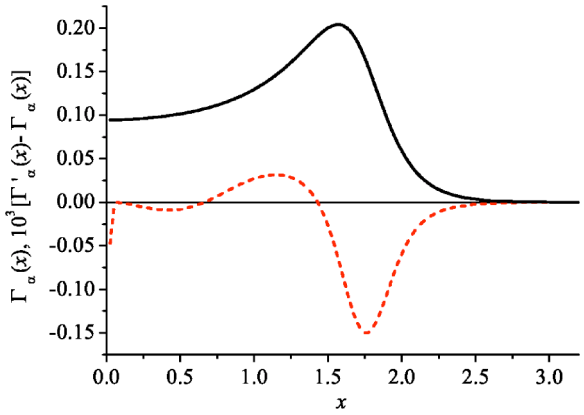

FIG. 4. Comparison of the approximation error $\Gamma'_\alpha(x) - \Gamma_\alpha(x)$ (dashed line, 1000 times magnified) with the function $\Gamma_\alpha(x)$ (solid line), for $\alpha = 1.5$.

III. RESULTS AND DISCUSSION

An example of a measured Thomson scattering spectrum is shown in Fig. 5. The plot covers the lower half (in the wavelength domain) of the Thomson spectrum taken 35 ns before the pinch, at a position horizontally 1.0 mm away from the center of the discharge, towards the source of the

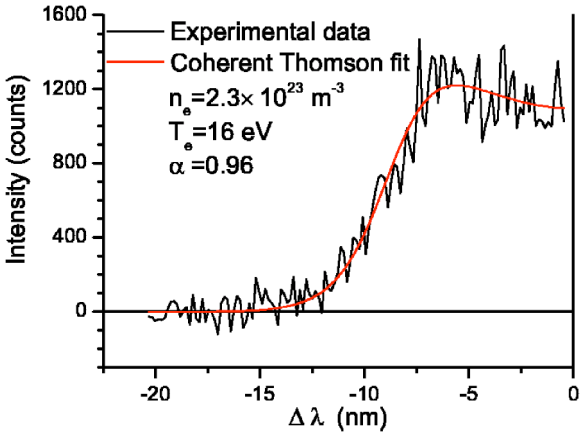

FIG. 5. Example of a measured TS spectrum. The negative counts at the lower wavelength end are due to the background subtraction. The smooth curve is a fit of the theoretical coherent-scattering spectrum to the experimental data. Fit results were $n_e = 2.3\times10^{23}$ m^{-3} and $T_e = 16$ eV, resulting in $\alpha = 0.96$.

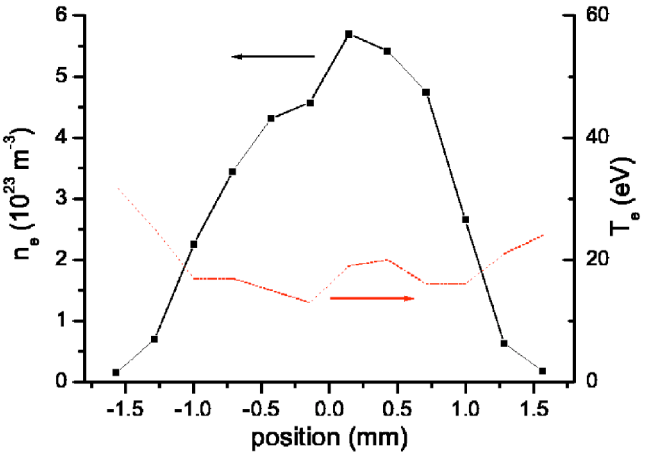

FIG. 6. Profiles of electron densities (symbols and solid curve) and electron temperatures (dashed curve) recorded 35 ns before the pinch.

TS laser pulse. The negative counts at the lower wavelength limit are due to the background subtraction.

For each measurement, five pixels on the CCD camera were grouped in the spatial direction to form "superpixels"; for each of these spatial positions, a fit of the Thomson spectrum was performed. An example of the resulting spatial profile is shown in Fig. 6. In some cases, especially at the edges of the plasma, the value of the fit parameter ξ was well below 1, meaning that the actual intensity of the Thomson signal, compared to the absolute calibration, was substantially lower than the one that would correspond to the fitted plasma parameters n_e and T_e. This is an indication of spatial and/or temporal gradients in the plasma, or pulse-to-pulse fluctuations of the discharge: apparently a plasma with certain density and temperature was present at the probed position, but only in a certain fraction of the volume, gate time, or of the number of pulses used in the integration. This fraction is reflected in the ratio of measured and expected signal intensity. The effective electron density, as plotted in Fig. 6, is the fit result multiplied with this fraction.

The electron temperature in Fig. 6 has a hollow spatial profile. A similar shape of the profile was observed in most of the other measurements during the prepinch phase. Near the boundaries between the plasma and the surrounding vacuum, the ion densities will be lower than in the center of the plasma. This is confirmed by the electron densities presented here, combined with the assumption of quasineutrality of the plasma. Hence, in the outer regions the electrons will undergo fewer collisions with other species in which they can lose their energy. Therefore, a certain Ohmic heating of the electrons will lead to higher electron temperatures here than in the central part of the cross section.

For each time step, the spatial maximum of the fitted electron density has been selected and a weighted average over the profile has been calculated for the electron temperature (the weight being the effective local electron density). Both have been plotted against time in Fig. 7.

The electron densities in the prepinch phase were found to increase from roughly $n_e = 10^{23}$ m^{-3} to 10^{24} m^{-3} in a time of about 100 ns, while the electron temperature increased from

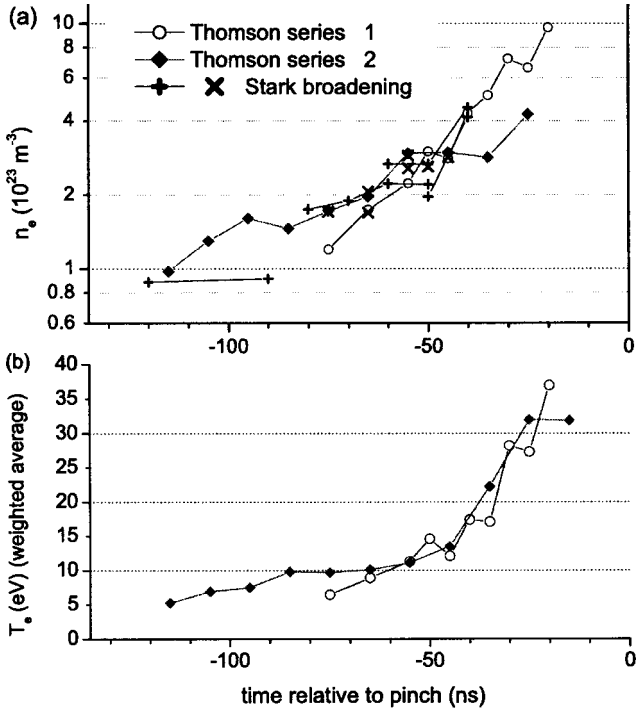

FIG. 7. Maximum fitted electron density for each profile [part (a)] and spatially averaged electron temperature weighted by electron density [part (b)] from Thomson scattering plotted as a function of time before the pinch. In part (a), results from Stark broadening measurements have been included for comparison.

some 5 eV to about 35 eV. The plasma radii in the prepinch and pinch phases can be estimated from the TS electron density profile widths and plasma imaging in the EUV [4], respectively. Given the electron densities in the prepinch phase, and comparing the plasma radius with the final radius in the pinch phase, one can derive that in the pinch, the electron density should reach a value of just over 10^{25} m^{-3}, assuming that the average ionization degree does not change much anymore during the compression.

As mentioned already in the Introduction, some line radiation was also detected in the plasma background during the prepinch phase. Using the Stark broadening effect, electron densities could be calculated from the linewidths. For one line, the $6d\ ^2D_{3/2} \rightarrow 6p\ ^2P^o_{1/2}$ Sn II line at 533.39 nm, the Stark broadening parameter was known from the literature [10,11]. The width of this line was used to cross-calibrate the Stark widths of three Sn III lines in the same spectral range. The method could thus be extended to higher densities and higher temperatures, at which the Sn^+ ion was absent. Electron densities derived using this method have been included for reference in Fig. 7. The figure shows that there is excellent agreement to within experimental error for both the magnitude and the trend of both sources of electron density information. Only at −90 ns is the TS result considerably larger than the Stark broadening result. A more elaborate discussion of the Stark broadening measurements will be given in a future publication.

Special care has been taken to evaluate the heating of the plasma, and more specifically of the electrons in the plasma, by the action of the laser. Nonlinear effects (such as multi-

photon or tunneling ionization) do not play a role under the moderate laser conditions as used in this work; under the present plasma parameters, the main absorption processes are inverse bremsstrahlung (IB), as described in [12–14], and absorption in spectral lines of low ionization stages of tin. The absorption coefficient for IB is given by

$$\kappa_{\mathrm{IB}} = \frac{\omega_{\mathrm{pl}}^2}{\tilde{n}(\omega_{\mathrm{laser}})c} \frac{\nu_{\mathrm{ei}}}{\omega_{\mathrm{laser}}^2 + \nu_{\mathrm{ei}}^2}, \tag{6}$$

where

$$\nu_{\mathrm{ei}} \approx \frac{1}{6\pi}\left(\frac{1}{2\pi m_e}\right)^{1/2}\left(\frac{1}{k_B T_e}\right)^{3/2} \frac{n_e Z e^4}{\varepsilon_0^2} \ln\sqrt{1+\Lambda^2} \tag{7}$$

and

$$\Lambda = \left(\frac{k_B T_e}{m_e}\right)^{1/2} \frac{4\pi\varepsilon_0 k_B T_e}{Ze^2} \frac{1}{\omega_{\mathrm{laser}}}, \tag{8}$$

in which ω_{laser} represents the laser angular frequency, ω_{pl} the plasma frequency, $\tilde{n}$ the refractive index (which is very close to 1 for the laser frequency and range of plasma parameters under consideration), ν_{ei} the electron-ion collision frequency for momentum transfer, and Z the average ion charge. Λ contains the laser angular frequency ω_{laser} rather than the plasma frequency ω_{pl}, as indicated in [13]. From κ_{IB}, the laser energy E_{laser}, the laser focal radius $r_0 \approx 200$ νm, and the electron density, an upper limit for the energy gained per electron can be derived under the assumption of absence of any loss channels. This leads to a maximum increase of the electron temperature given by

$$\Delta T_{e,\max} = \frac{2}{3}\frac{\kappa_{\mathrm{IB}} E_{\mathrm{laser}}}{k_B \pi n_e r_0^2}. \tag{9}$$

An estimate of the temperature increase averaged over the duration of the laser pulse (which is relevant for the Thomson scattered signal) was obtained by taking half of the total laser pulse energy, or about 80 mJ, for E_{laser}. An evaluation of Eqs. (6) and (9) using this energy shows that for the measurements presented in this paper, $\kappa_{\mathrm{IB}} \leqslant 0.08$ m^{-1} (assuming that $Z \leqslant 10$), so that $\Delta T_{e,\max}$ never exceeds 0.2 eV. For the first part of the prepinch phase, until 45 ns before the pinch, $n_e \leqslant 3\times 10^{23}$ m^{-3} and $T_e \leqslant 15$ eV so that $\Delta T_{e,\max}$ even stays below 0.05 eV. Therefore, inverse bremsstrahlung in all cases only leads to a very small relative error in the measured electron temperature. In the pinch phase, assuming $n_e \approx 1\times 10^{25}$ m^{-3}, $T_e \approx 30$ eV, and $Z \approx 10$, $\Delta T_{e,\max}$ would be about 2 eV.

Absorption of laser energy due to line transitions mainly plays a role in the relatively cool first part of the prepinch phase, when Sn^+ and Sn^{2+} are still abundant. Especially the Sn II line mentioned above will contribute to the absorption since it is sufficiently broadened for the wings of the line profile to reach to the laser wavelength at 532.0 nm. The effect of absorption and stimulated emission at the laser wavelength will be that the upper and lower levels of the transition become strongly coupled, so that their densities per statistical weight become nearly equal. The distribution function of the other excited states, which is assumed to be Boltzmann-like when absorption is absent, will also become disturbed. As a result of this, the ionization potential of Sn^+ will effectively get lowered by a certain fraction of the photon energy of 2.33 eV. This effect is illustrated schematically in Fig. 8. We estimated that in the most extreme case, the electron density will show an increase of about 30%. Indeed, we believe that the difference in Fig. 7 between Stark and Thomson results at 90 ns before the pinch can partially be explained by this effect.

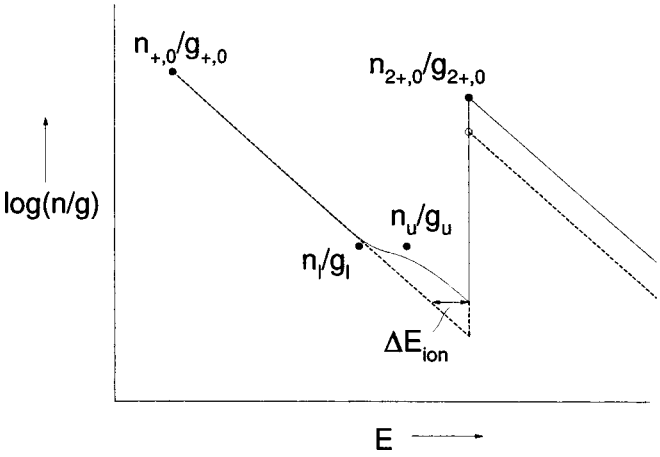

FIG. 8. A schematic plot of the excited states distribution function of the Sn^+ and Sn^{2+} systems in the presence of the laser field. Dashed line, undisturbed Saha-Boltzmann distribution; solid dots, densities per statistical weight of the lower and upper levels coupled by the laser field; solid line, approximate disturbed distribution. The densities in the plot are normalized to the density of the ground state of Sn^+. The effective lowering of the ionization energy of Sn^+ is indicated by the horizontal arrow. See the text for further explanation.

A second result of the disturbed distribution function is that electronic deexcitation from the upper level to the lower level will happen more frequently than electronic excitation from the lower to the upper level. Because the free electron loses energy in the electronic excitation process and gains energy in the reverse process, the imbalance will lead to a net heating of the free electrons in the plasma. We used a simple stationary-state collisional radiative model similar to the one described in [15], and the following expression for the approximate collisional (de)excitation rates as used in [16,17], to evaluate the order of magnitude of this effect,

$$X(T_e,l,u) = \frac{6\times 10^{-12} f(l,u)}{\Delta E\sqrt{T_e}} \exp\left(\frac{-\Delta E}{T_e}\right),$$

$$X(T_e,u,l) = \frac{g_l}{g_u}\frac{6\times 10^{-12} f(l,u)}{\Delta E\sqrt{T_e}}. \tag{10}$$

Here, l and u denote the lower and upper states of the transition, and ΔE is the energy difference between both states in eV. The oscillator strength $f=0.73$ was derived from the optical transition probability of the Sn II line, $A=8.6\times 10^7$ s^{-1}, as given by [18]. We found that the line absorption of laser light might lead to an increase of the electron temperature of up to a few eV in the most extreme case, and only when Sn^+

is the dominant ion. Later in the prepinch phase the average charge of the ions will have increased to higher values, so that the Sn^+ and Sn^{2+} ions are no longer abundant. At that time, heating and ionization by line absorption will not be important any longer.

It is worth noting that both effects are virtually *independent* of the laser power, as long as the power is large enough to disturb the Boltzmann distribution of the excited states of Sn^+. However, the increase of electron temperature does depend linearly on the pulse *duration*.

From extrapolation of the measured Thomson scattered intensities to the expected electron temperatures and densities in the trigger and pinch plasma phases of the discharge, and comparison with the levels of background radiation measured for those phases, it was found that the peak intensity of the Thomson spectrum would amount to only 2% and 3%, respectively, of the intensity of the background. During the trigger phase, the background consists mainly of line radiation, while during the pinch phase it forms a (quasi)continuum. In both cases, pulse-to-pulse fluctuations in the background emission render the accurate determination of the Thomson signal impossible under the present experimental limitations.

IV. CONCLUSIONS AND FUTURE WORK

In this work, the feasibility of Thomson scattering on actual EUV producing plasmas has been proven. Electron densities in the prepinch phase have been found to increase from about 10^{23} m^{-3} to near 10^{24} m^{-3}, while simultaneously the electron temperature increased from around 5 eV to more than 30 eV. The increase in the electron density can be explained both by the first onset of the plasma compression, and by a strong increase of the ionization degree of the plasma due to the increasing electron temperature.

It has been shown that the heating of the plasma by means of inverse bremsstrahlung absorption of the TS laser pulse does not significantly affect the results. In the very beginning of the prepinch phase, absorption of laser light in line radiation may be the cause of a certain overestimation of both the electron density and the electron temperature. The line absorption could lead to an increase of electron density of about 30%.

For the largest part of the prepinch phase, measurements of the electron densities using the Stark broadening of tin lines in the plasma confirm both the magnitude and the trends in the TS data.

The present experiments have also shown that the applicability of Thomson scattering to the very early part of the discharge, and the pinch and decay plasmas, is limited due to an excessively high level of background radiation (formed by line radiation, a quasicontinuum, and again line radiation, respectively). Efforts are underway to come to the necessary adjustments of the setup that will make sub-ns experiments possible. These include the application of a stimulated Brillouin scattering (SBS) cell to compress a laser pulse to sub-ns duration, and a sub-ns gated ICCD camera that is properly synchronized to the TS laser light pulse. The better signal-to-background ratio will enable probing the remaining discharge phases. The theory shows that the shorter pulse length will help to reduce the increase of electron temperature due to absorption in spectral lines. Also, measurements as a function of laser pulse energy will become possible, so that the assumptions about the laser-induced plasma heating in the pinch phase can be checked experimentally.

[1] *Proceedings of the EUV Source Workshop*, International SEMATECH, Antwerp, Belgium, 2003, edited by V. Bakshi (unpublished).

[2] E.R. Kieft, J.J.A.M. van der Mullen, G.M.W. Kroesen, and V. Banine, Phys. Rev. E **68**, 056403 (2003).

[3] E.R. Kieft, J.J.A.M. van der Mullen, V. Banine, K. Koshelev, and G.M.W. Kroesen, in *Proceedings of the EUV Source Workshop*, International SEMATECH, Antwerp, Belgium, 2003, edited by V. Bakshi (unpublished).

[4] E.R. Kieft, J.J.A.M. van der Mullen, G.M.W. Kroesen, V. Banine, and K.N. Koshelev (unpublished).

[5] M.J. van de Sande, Ph.D. thesis, Eindhoven University of Technology, 2002, http://alexandria.tue.nl/extra2/200210414. pdf.

[6] M.J. van de Sande and J.J.A.M. van der Mullen, J. Phys. D **35**, 1381 (2002).

[7] M.J. van de Sande, R.H.M. Deckers, F. Lepkojus, W. Buscher, and J.J.A.M. van der Mullen, Plasma Sources Sci. Technol. **11**, 466 (2002).

[8] X. Zhu, M. Redwitz, E.R. Kieft, M.J. van de Sande, and J.J.A.M. van der Mullen J. Phys. D **37**, 736 (2004).

[9] E.E. Salpeter, Phys. Rev. **120**, 1528 (1960).

[10] M.H. Miller, R.A. Roig, and R.D. Bengtson, Phys. Rev. A **20**, 499 (1979).

[11] Be. Martínez and F. Blanco, J. Phys. B **32**, 241 (1999).

[12] T. Hughes, *Plasmas and Laser Light* (Adam Hilger, Bristol, 1975).

[13] T. Johnston and J. Dawson, Phys. Fluids **16**, 722 (1973).

[14] K. Garloff, M. van den Donker, J.J.A.M. van der Mullen, F. van Goor, R. Brummans, and J. Jonkers, Phys. Rev. E **66**, 036403 (2002).

[15] D. Colombant and G.F. Tonon, J. Appl. Phys. **44**, 3524 (1973).

[16] A.C. Kolb and R.W.P. McWhirter, Phys. Fluids **7**, 519 (1964).

[17] R. W. P. McWhirter, in *Plasma Diagnostic Techniques*, edited by R. H. Huddlestone and S. L. Leonard (Academic, New York, 1965).

[18] W.L. Wiese and G.A. Martin, *Wavelengths and Transition Probabilities for Atoms and Atomic Ions, Part II: Transition Probabilities* (U.S. National Bureau of Standards, Washington, D.C., 1980).